BEAM DYNAMICS OF THE CRNL SUPERCONDUCTING CYCLOTRON EXTRACTION SYSTEM

E.A. Heighway and C.R. Hoffmann
Atomic Energy of Canada Limited, Research Company
Chalk River Nuclear Laboratories
Chalk River, Ontario, Canada K0J 1J0

Summary

The extraction system for the Chalk River superconducting cyclotron consists of a single electrostatic deflector followed by a series of magnetic elements. These employ both passive iron elements and superconducting windings that provide variable deflection and focusing to extract all ions with acceptable beam growth and phase space distortion and with no physical motion of any components. Calculations done to analyze the performance of this system are described. Included is a description of the treatment of the field map data used for both the main magnetic field and for the channel elements. The beam dynamics for several ions in the extraction channel are described in detail.

Introduction

The extraction system for the Chalk River superconducting cyclotron remains fundamentally unaltered since its original conception[1]. However within the magnetic channel elements[2] the coil geometry and conductor type have changed and these are described in detail elsewhere[3].

The system, which is shown in Fig. 1, consists of an electrostatic deflector located in a dee followed by a series of fixed-position magnetic elements. The latter consist of two lens sections and two magnetic channels. Figure 2 shows the layout of the system along the beam path and identifies the nature and function of each element. The deflector provides variable steering at up to 140 kV/cm. The lens sections are saturated iron elements providing fixed steering and fixed focusing. Channel 1 combines fixed focusing from saturated iron with variable steering from superconducting coils. Channel 2 uses superconducting coils to provide variable focusing and variable steering with the latter independently variable in each of the two halves of the channel.

In the sections which follow the generation of the maps of magnetic induction required by the beam dynamics codes and the procedures used to track the particles into and through the extraction system are described. The performance of the system is illustrated by showing the beam dynamic properties of a few ions.

Magnetic Induction Data

The essential raw material for the extraction calculations is the midplane magnetic induction along the extraction path. This induction is generated by the cyclotron steel and main coils and by the individual extraction channel elements.

The cyclotron midplane induction has been measured and is accurately known[4] only at locations radially inside the cryostat (shown as B in Fig. 1). Beyond this mapped region, out to the yoke wall, induction data were taken with a single flip coil[5] along lines through the injection hole D and the probe hole C. No access was available to the extraction region.

In modeling the extraction system the induction data used to represent this outer region has therefore been calculated. The calculation accuracy is known to be high from the earlier comparison with measurements[4], with the largest errors being close to the flutter poles. Further out, beneath the coils where the contribution from the steel is reduced the accuracy will be higher. To make use of this information the calculated induction in the outer region has been modified by application of a rapidly radially decreasing empirical correction which also varies with azimuth. This results in the calculated induction blending smoothly with the accurately measured induction in the inner region.

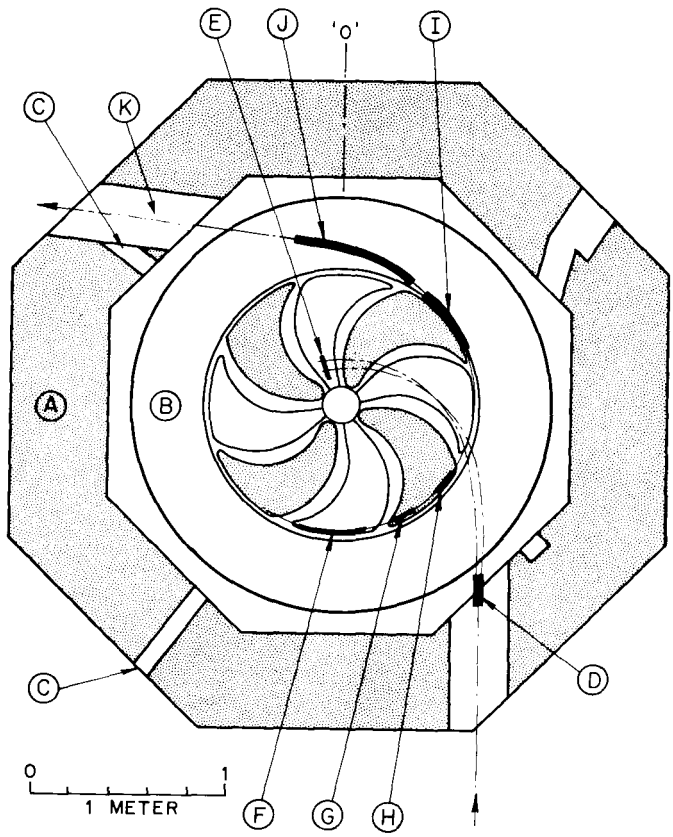

Fig. 1 Midplane plan view of the cyclotron: A - yoke; B - cryostat; C - diagnostic probe holes; D - injection steering dipole; E - stripper foil; F - electrostatic deflector; G,H - magnetic lens sections; I,J - magnetic channel 1 and 2; K - extraction yoke hole.

Near the yoke wall the effects of the holes penetrating the yoke become important and as these were not part of the original calculation, special attention was given to calculating the induction perturbations they produce. To do this the holes have been modeled in the uniform magnetization approximation assuming the yoke magnetization $\underline{M}$ was axial and uniform so that the perturbations could be represented as if from the equivalent surface current density $\underline{K} = \underline{M} \times \underline{n}$ as shown in Fig. 3. At low induction this approximation is less valid but still gives a reasonable representation of the distribution if not the magnitude. The injection hole flip coil induction measurements were used to normalize the calculated induction to agree with that measured in the yoke holes by calculating an effective M. This effective

CH1996-3/84/0000-0141 $1.00 © 1984 IEEE

magnetization is plotted in Fig. 4 against the magnet central azimuthally averaged induction and shows that the perturbing effect of the yoke holes falls off rapidly with decreasing induction and will be negligible at the lowest operating induction of 2.5 T.

The induction generated by the iron and superconducting coils of the channel elements has to be calculated. The iron has been entirely represented using the uniform magnetization approximation which is very good since the iron is in an axial induction never less than 2 T. The midplane induction from the coils was calculated by a Biot-Savart integration but to calculate the winding end effects and the position of maximum induction (critical current) precisely, the code GFUN[6] was used. The induction from the channel elements is simply superposed with the calculated main magnet induction.

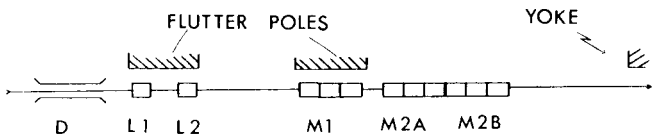

DEFLECTOR (D)	LENS (L1,L2) SECTIONS	MAGNETIC CHANNEL SECTIONS (M1, M2) (EACH HAS THREE MODULES AS SHOWN)	
ELECTROSTATIC DEFLECTION	SATURATED IRON	SATURATED IRON PLUS SUPERCONDUCTING WINDINGS	SUPERCONDUCTING WINDINGS
VARIABLE STEERING	FIXED STEERING FIXED FOCUSING	VARIABLE STEERING FIXED FOCUSING	VARIABLE STEERING IN 2A AND 2B VARIABLE FOCUSING BUT 2A, 2B SAME

Fig. 2 Schematic layout of the extraction system showing the nature and function of each element.

The iron elements in the extraction system produce large harmonic imperfections in the accelerating region. To reduce these, iron compensating elements located diametrically opposite the channel elements have been used. These elements, also included in the induction maps, reduce the first harmonic induction imperfection to less than 0.1 mT throughout the acceleration region.

Orbit Code Development

A fundamental consideration in the extraction system design has been the orbit dynamics and in preparation for commissioning the cyclotron there has been considerable development of the code used for accelerated beam dynamics including extraction.

The code SUPERGORLIN (developed from a version of GORLIN obtained from TRIUMF) has now been refined to allow inclusion of the measured inner and calculated outer maps of the cyclotron main magnet, the perturbations from the yoke holes and all the inductions from the saturated iron and superconducting coils of the magnetic channels. As well as these data handling provisions, major improvements now allow the code to optimize cyclotron parameters. Two important examples are (a) the ability to determine automatically the external beam parameters necessary at injection to center and phase the orbits beyond the internal stripper foil correctly and (b) the ability to thread the beam automatically through the extraction channel to the extraction port in the yoke. Both of these would otherwise require tedious searching and tuning.

Another important enhancement now permits a second order transfer matrix between several locations in the cyclotron to be calculated. This was essential in the injection beam line design where the cyclotron was represented by its transfer matrix in the code TRANSPORT[7]. This enhancement has proved important to the extraction calculations where the same algorithms were used to allow generation of precise transverse phase space plots. Previously Δr, Δp_r plots were used to represent transverse phase space along the injection and extraction paths.

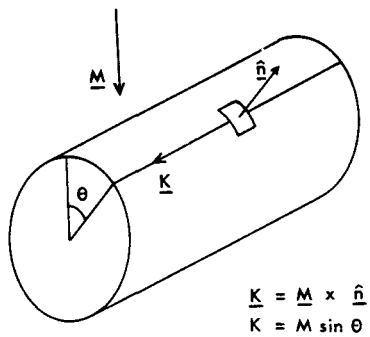

Fig. 3 The holes through the yoke wall were modeled assuming the yoke was uniformly magnetized with magnetization M. The perturbation in induction was calculated from the equivalent surface current density K.

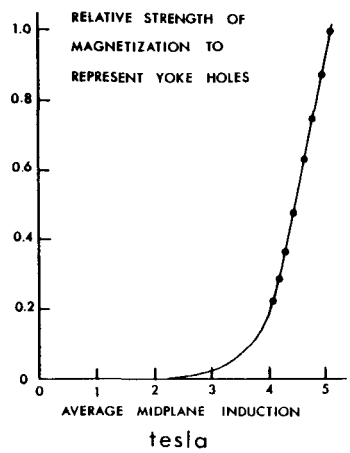

Fig. 4 Effective magnetization used in the calculation of the perturbations due to holes in the yoke wall as a function of midplane induction. (Based on flip coil measurements in the injection hole.)

The Extraction Calculations

The extraction calculations have sought to simulate as closely as possible what we expect to see with our first beams. The first step in the extraction calculation is injection, to determine as accurately as possible those injection beam parameters (immediately after beam stripping at the foil at the cyclotron center) which result in a well centered beam being accelerated out to the extraction radius. Once this has been achieved a first harmonic field perturbation provided by an azimuthal variation in the outermost trim rod settings is used to increase (by the precessional technique) the turn separation at the electrostatic deflector to 5 mm or greater. Simultaneously, small adjustments are made to the dee

CH1996-3/84/0000-0142 $1.00 © 1984 IEEE

voltage to center the last turn on the deflector entrance. Further adjustments will ultimately be necessary to centre the beam along the deflector to maximize beam clearance. This is then followed by the automatic threading of the beam down the extraction system (see Fig. 2) by: varying the deflector volts to enter magnetic channel 1, varying channel 1 bias to enter channel 2A, varying channel 2A bias to enter channel 2B and finally varying channel 2B bias to reach the yoke wall exit port.

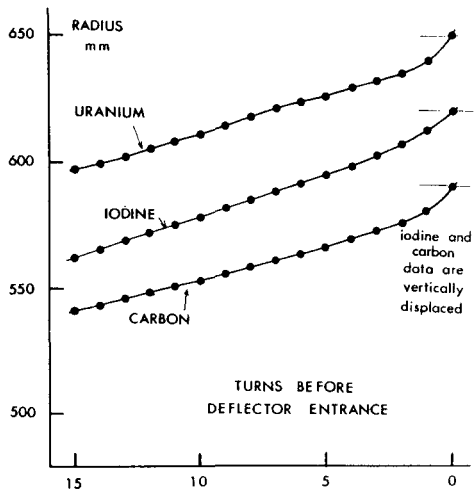

Fig. 5 Radial position of last turns before extraction showing the increased turn separation at the last turn.

Once the channel settings are determined a cluster of particles lying on the surface of phase space projection ellipses of the beam at injection can be transported from injection to extraction. The only remaining adjustment is that of channel 2 gradient to obtain optima in both transverse phase spaces at the cyclotron exit port. This single freely variable focusing element (channel 2 gradient) is sufficient to match all beams. This is because most of the radial defocusing is produced by the gradient at the outer flutter pole edge which does not depend strongly on midplane induction and is largely compensated by the fixed gradients provided by the iron in the lens and channel 1 sections. The required compensation is therefore much the same for all ion species.

The Beam Dynamics

The performance of the extraction system is illustrated by the dynamics of three ions - 23 MeV/u carbon 5^+, 10 MeV/u iodine 23^+ and 10 MeV/u uranium 33^+. Figure 5 shows the radial position of the last few turns for each ion and the precessional turn separation enhancement. Figure 6 shows the radial and axial transverse phase space plots as a function of position along the extraction system. In each case the starting transverse phase space coordinates were those corresponding to best estimates of expected emittance for each ion matched to minimize betatron oscillation amplitudes at injection.

Figure 7 shows maximum transverse beam sizes along the channel including for uranium the effect of mistuning the channel 2 gradient coils. Figure 8 shows the small differences in trajectory of the three ions as a function of path length. Table 1 shows the extraction system parameters necessary to extract the three ions.

Table 1

Extraction System Parameters

Ion	23MeV/u Carbon 5+	10Mev/u Iodine 23+	10Mev/u Uranium 33+
Deflector Gradient (kV/cm)	68.1	69.7	126.7
Lens 1 Gradient (T/m)	25.9 (*)		
Lens 2 Gradient (T/m)	26.0 (*)		
Channel 1 Bias (T)	0.398	0.079	-0.246
Channel 1 Gradient (T/m)	36.2 (*)		
Channel 2A Bias (T)	0.186	0.196	0.280
Channel 2 Bias (T)	0.365	0.220	0.120
Channel 2 Gradient (T/m)	10.0	10.0	15.0

(*) Fixed

Acknowledgements

Thanks are due to Mike Coulas and Steve Keyes for their work on the orbit codes, to John Ormrod for helpful discussions and the injection emittance and stripping data, and to Margaret Trecartin for her untiring efforts on the manuscript.

References

1. C.R. Hoffmann, IEEE Trans. Nucl. Sci., NS-24 (3), 1470 (1977).
2. C.R. Hoffmann, Proc. Ninth Int. Conf. Cyclotrons and Their Application, Caen, France (1981), Les Editions de Physique, p. 497.
3. C.R. Hoffmann, J.F. Mouris and D.R. Proulx, "Design and Test of Prototype Superconducting Extraction Channel Modules for the Chalk River Superconducting Cyclotron", these proceedings.
4. J.H. Ormrod et al., IEEE Trans. Nucl. Sci., NS-26 (2), 2034 (1979).
5. J.H. Ormrod, Atomic Energy of Canada Limited, Report AECL-7842 (1982).
6. A.G.A.M. Armstrong et al., "GFUN3D User Guide", 2nd edition, RL-76-029, Rutherford Appleton Laboratory (1979).
7. K.L. Brown et al., "TRANSPORT, A Computer Program for Designing Charged Particle Beam Transport Systems", SLAC-91, Rev. 2, UC-28, Stanford Linear Accelerator Center (1977).

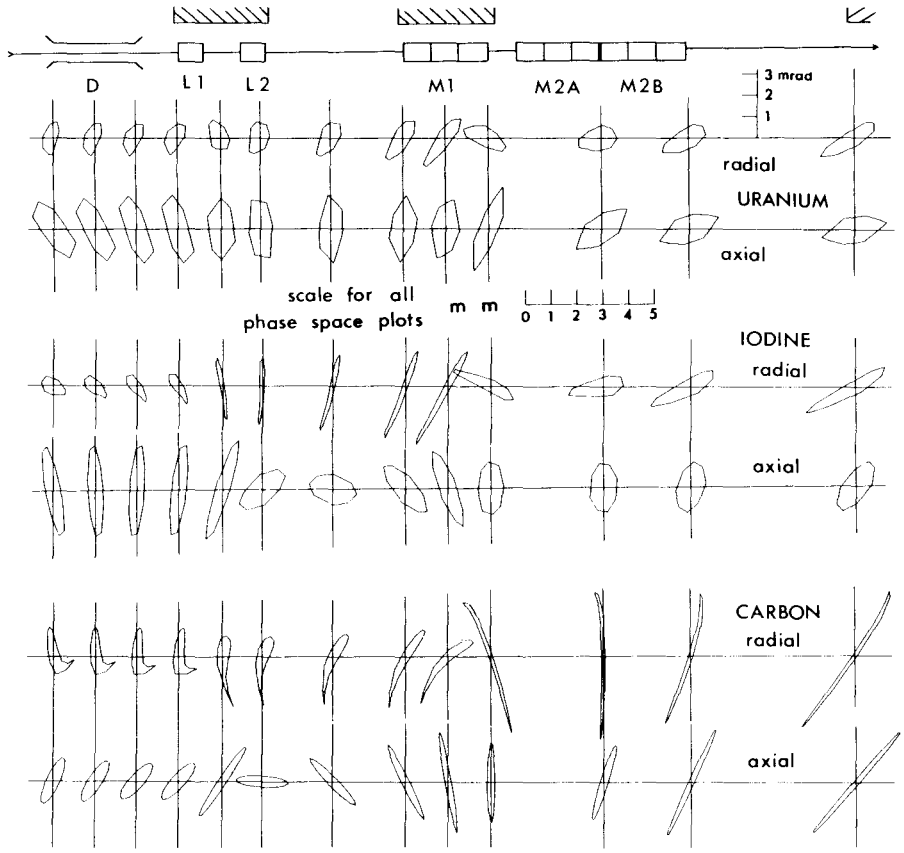

Fig. 6 Radial and axial phase space plots along the extraction system for the three ions 10 MeV/u uranium 33^{+}, 10 MeV/u iodine 23^{+} and 23 MeV/u carbon 5^{+}.

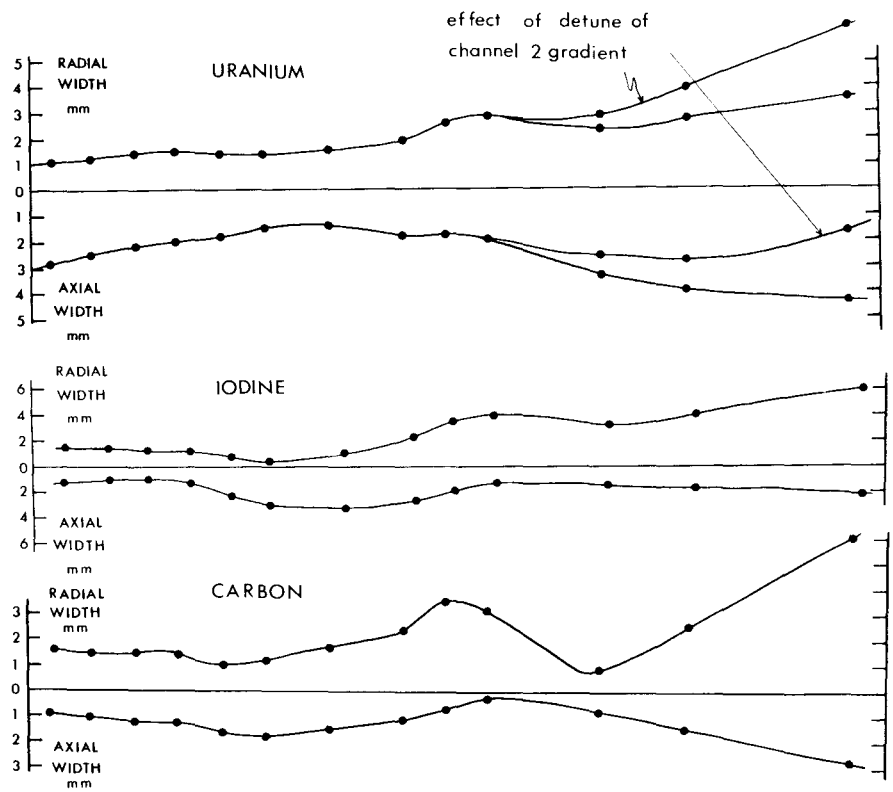

Fig. 7 Radial and axial beam envelope full width along the extraction system for the three ions. For the uranium ion the effects of channel 2 gradient mistuning have been shown.

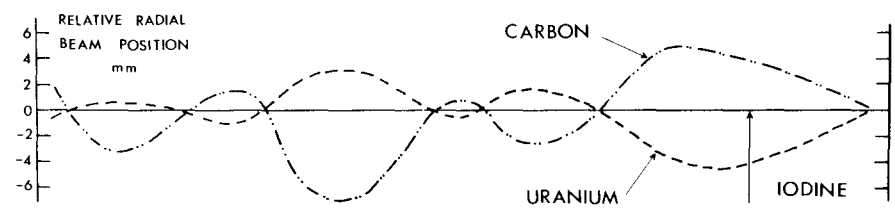

Fig. 8 The radial displacement of the beam centroid for the three ions along the extraction system relative to that of the iodine beam which is the reference trajectory.